Polarization Sensitive QWIP Thermal Imager

March 2000

Daniel W. Beekman
Army Research Laboratory, AMSRL-SE-EE
2800 Powder Mill Road, Adelphi, MD 20783-1197

James Van Anda
Digital Imaging Infrared, Inc.
174 Semoran Commerce Place, Suite 111, Apopka, FL 32703

ABSTRACT

A polarization-sensitive thermal imager has been assembled using a quantum-well infrared photodetector (QWIP) focal plane array (FPA) with peak responsivity in the long-wave infrared (LWIR) spectral band near 9 μm. Polarization-dependent responsivity is achieved by etching linear gratings onto each pixel during QWIP FPA fabrication, with adjacent pixels having orthogonal grating orientation. The direct integration of the gratings with the pixels eliminates all pixel registration errors encountered with previous infrared polarimetry instruments. We present here details of the FPA and thermal imaging system design and performance and show examples of polarization-enhanced imagery.

1. Introduction

Exploitation of infrared polarization signatures can enhance the contrast of targets vs backgrounds. Targets are composed of man-made materials that tend to be smoother than natural materials, and hence both reflect and emit a stronger polarization signature than natural backgrounds.

The development of polarization-sensitive infrared detectors is complex. Some previous efforts have employed rotating polarizers [1], polarization elements at an intermediate focal plane [2], and a polarization beam splitter producing two images on a single FPA [3]. The practical use of such instruments also involves added complexities [4]. Polarization analysis is very sensitive to misalignments, and precise six-axis alignment is difficult to achieve, verify, and maintain.

We have designed and fabricated a focal-plane array (FPA) detector with polarization elements integrated onto each pixel, which eliminates the alignments and artifacts associated with separate polarization elements or multiple images. A description of the instrument and some preliminary characterization data is given below.

Report Documentation Page

Report Date	Report Type	Dates Covered (from... to)
00032000	N/A	-

Title and Subtitle Polarization Sensitive QWIP Thermal Imager	**Contract Number**
	Grant Number
	Program Element Number
Author(s) Beekman, Daniel W.; Van Anda, James	**Project Number**
	Task Number
	Work Unit Number
Performing Organization Name(s) and Address(es) Army Research Laboratory, AMSRL-SE-EE 2800 Powder Mill Road Adelphi, MD 20783-1197	**Performing Organization Report Number**
Sponsoring/Monitoring Agency Name(s) and Address(es) Director, CECOM RDEC Night Vision and Electronic Sensors Directorate, Security Team 10221 Burbeck Road Ft. Belvoir, VA 22060-5806	**Sponsor/Monitor's Acronym(s)**
	Sponsor/Monitor's Report Number(s)
Distribution/Availability Statement Approved for public release, distribution unlimited	
Supplementary Notes	
Abstract	
Subject Terms	
Report Classification unclassified	**Classification of this page** unclassified
Classification of Abstract unclassified	**Limitation of Abstract** UNLIMITED
Number of Pages 11	

2. QWIP FPA Processing

Quantum well infrared photodetectors (QWIPs) are composed of multiple thin layers of III-V semiconductor materials, e.g. GaAs and $Ga_{1-x}Al_xAs$ [5-7]. A fundamental characteristic of QWIPs is that infrared radiation will be absorbed and detected only if there is an electric field component perpendicular to the layers. A standard QWIP is made with a grating on each pixel to diffract incident IR radiation into a direction nearly parallel to layers, so the electric field vector is nearly perpendicular to the layers. To maximize the detectivity, a square grid grating – equivalent to two orthogonal linear gratings – is typically used to detect all linear polarization orientations. Note that QWIP cameras have also been demonstrated in the mid-wave infrared (MWIR: 3-5 μm) spectral band, and vertically-integrated dual-band QWIP cameras have been demonstrated in various combinations: MWIR/LWIR (using rectangular grid gratings), MWIR/MWIR, and LWIR/LWIR.

The FPA described here was fabricated with a linear grating on each pixel, and with orthogonal grating orientations on adjacent pixels. Figure 1 shows our FPA after the grating etch and before the deep etch between pixels. Because the refractive index of GaAs is approximately 3, the 3-μm period of the grating is appropriate for a detector with peak response wavelength near 9 μm. The spectral width is about 1.5 μm FWHM, and the total size of the FPA is 288 x 384 pixels with a 40-μm pixel pitch.

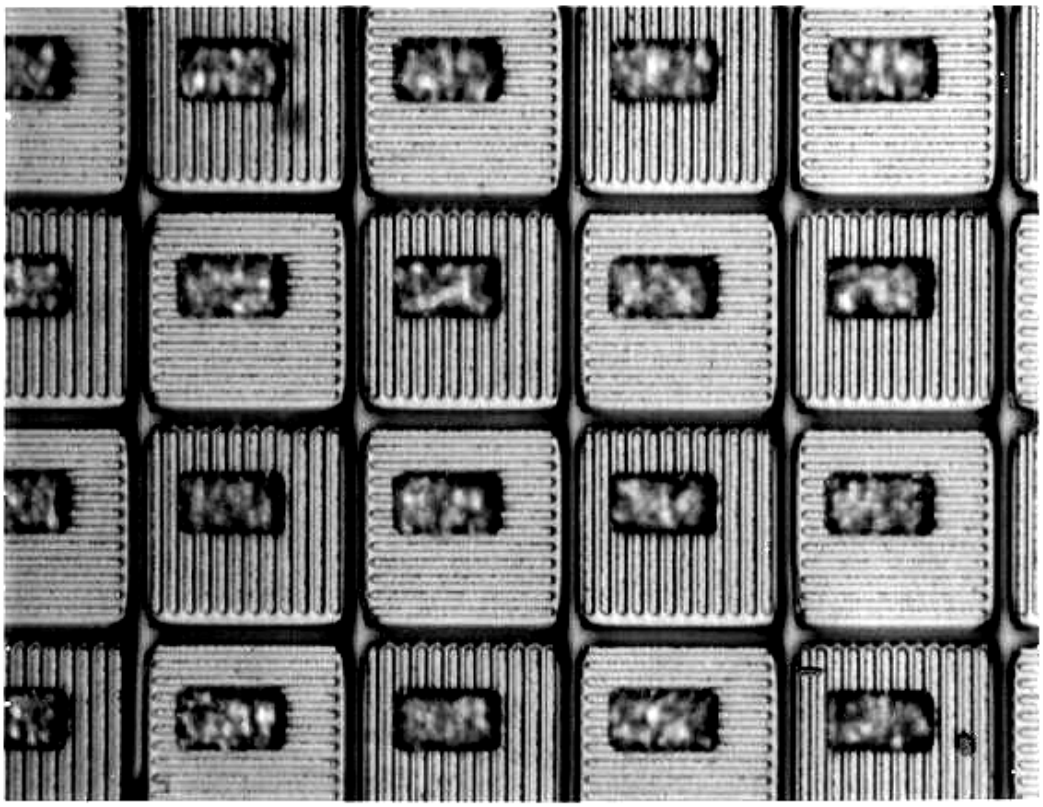

Figure 1. Micrograph of etched gratings in a 288 x 384 array. The gratings have a 3 μm period, and the pixel pitch is 40 μm.

A camera based on this FPA could be operated in either staring mode and microscan mode. The staring mode would be appropriate for well-resolved targets, in which adjacent pixels would simultaneously image adjacent portions of a single target facet. Alternatively, a microscan mechanism would allow adjacent pixels to view the same portion of the target in successive frames. For the test results presented here, the staring mode was used exclusively.

3. Electronics

The DI 9800 QW is an infrared thermal imaging sensor including electronics, detector, and lens. The system is designed for use with the polarized QWIP technology. The unit is controlled by digital and analog interfaces and can also be controlled remotely using an RS-232 link.

Functional Interfaces

The DI 9800 QW has the following operating modes and controls. These functions are controlled locally or by an RS-232 Serial Control Link:

i.	Display polarity	white hot/black hot
ii.	Focus direction	near/far
iii.	Level mode	automatic/manual
iv.	Manual gain command	0 db to +12 db
v.	Manual level command	full black to full white
vi.	Freeze Frame	on/off
vii.	Power	on/off
ix.	Gray scale	on/off
xi.	Built-In Test (initiated)	

RS-170 Compatible Video Out
12-Bit Digital Video Out

Major Components List

The DI 9800 QW system block diagram is shown in Figure 2. The imager contains the following seven major components:

a. Detector Buffer Circuit Card Assembly (CCA)
b. FLIR Processing CCA
c. Video Processing CCA
d. Power/Controls CCA
e. Focus Lens Assembly
f. Polarized QWIP Detector/Cooler
g. Software

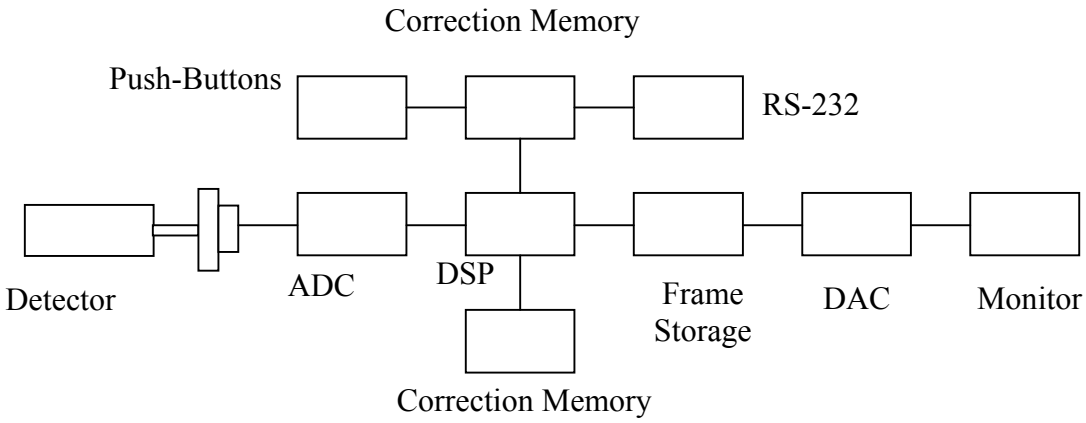

Figure 2. Block diagram of DI-9800-QW system.

Detector Buffer CCA

The Detector Buffer CCA is a small electronics assembly and interfaces to the detector pins. This assembly contains the detector drive electronics, the power sequencing switches and noise filters, the clock and strobes recievers, and the detector output amplifiers and cable driver.

FLIR Processor CCA

The FLIR Processor CCA supports the nonuniformity correction, global gain and level control, failed pixel substitution, dynamic range reduction, BIT status and serial link command processing. An integrated processor or DSP is used to support these functions. All operational software is stored in nonvolatile memory and run from RAM. The processor CCA also has a high speed 14 bit data acquisition A/D converter.

Video Processor CCA

The Video Processor CCA supports all the digital image enhancement processing including dynamic range reduction, Geometric distortion correction, etc. This CCA generates the RS-170 timing signals and provides external video synchronization capability. There is limited symbology to provide key status and operator feedback. A 256K x 16 dual ported RAM is used to implement video storage and symbology.

This provides three levels of symbology intensity from black to white. The CPU interfaces with the symbology to load one plane without affecting the symbols on the other planes.

Through a serial command, the gray scale test pattern can be displayed. The gray scale is made of ten equal steps from black to white (white = maximum video). The 10 steps are equally spaced horizontally and on the bottom sixty lines of the raster with the rest of the raster having normal video.

The analog video output is provided by this CCA. The video is filtered by a low pass filter to minimize noise and clock signal feedthrough from degrading the system NEΔT and MRTD performance. After filtering, the video is terminated in 75 ohms. Video outputs are available to drive a 75-ohm load with a 1 volt peak-to-peak composite video signal.

Power Supply

The Power Supply needed for operation of the DI 9800 QW is +12 volts. This supply should be capable of supplying 12 watts of power. The power lines are well-filtered within the DI 9800 QW. Low frequency hum and noise should be limited to less than 100 mv peak-to-peak.

Dynamic Range

The dynamic range of the DI 9800 QW is 14 bit input signal. The internal arithmetic is done in 32 bit fixed point notation. Coefficient tables are 16 bit wide for both gain and level. The implementation of the system correction algorithm follows the dynamic range of the input signal 14 bits.

Uniformity

Fixed pattern noise is the result of errors in the input reference frame from which the coefficients are calculated. The reference input frames are usually averaged to reduce the noise, which also reduces the reference errors. The algorithm in the DI 9800 Engine allows the user to select the number of frames to average.

Sensitivity

The sensitivity for full video with maximum gain referenced to a 300 K background is normally set to be $4^{o}C\ \Delta T$.

Gain and Level Control

The DI 9800 QW shall provide for automatic or manual level control. The mode of operation shall be selected by the Control Panel. In the manual mode, the gain has 16 bits of resolution and the level has 16 bits of resolution.

Nonuniformity Correction (NUC)

Nonuniformity correction coefficients are saved in 512 K of 16-bit nonvolatile memory.

Video Output Definition

The DI 9800 Engine shall supply a composite video output compatible with standard RS-170:

a. Signal Impedance: 75 Ω
b. Signal Amplitude: 1v peak-to-peak
c. Normal pedestal
d. Signal horizontal frequency: 15,734.264Hz ±l.0 Hz

Initiated Built in Test (BIT)

The DI 9800 QW shall provide user-initiated or power-up BIT. At initial power-up or for user-initiated BIT, the software is responsible for executing the following tests.

a) DSP RAM test
b) Nonvolatile checksum verification
c) CCA level digital pattern injection test
d) Power voltage limits test

4. Camera Integration

The electronics used on the Polarization Sensitive Thermal Imager is the standard Digital Imaging DI-9800 electronics set shown in Fig 3. The imaging processor generates the timing signals to correctly operate the multiplexer. It transmits the timing to the buffer CCA and receives an analog signal back. Nonuniformity correction is applied with coefficients that are computed during calibration and stored in the onboard RAM. Image enhancement, such as ordering the pixels as described below, is done and the pixel data is sent to the video card. The video card computes the output gray value and generates RS-170 compatible video.

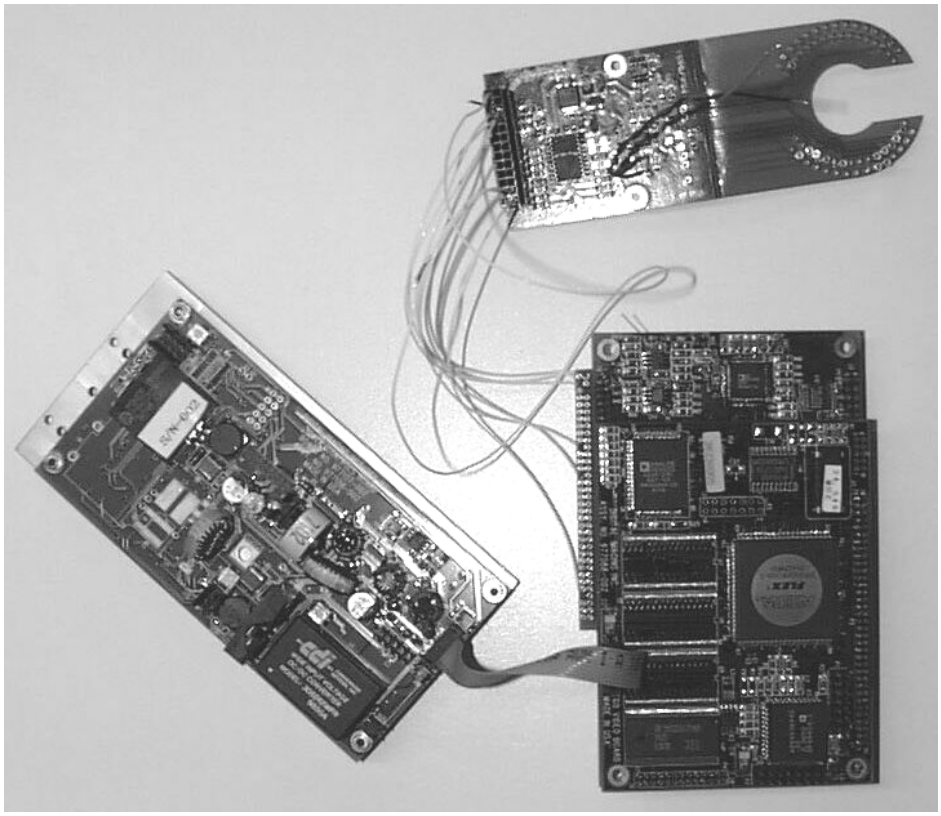

Figure 3. Digital Imaging DI 9800 electronics set.

A 320x240 horizontally polarized and a 320x239 vertically polarized picture is generated from the detector array. The elements on the FPA are arranged in a diagonal pattern as shown in Fig. 1. A typical read out sequence (for example the horizontally polarized pixels) is shown in Fig.4. The first line reads pixel 1 from row 1 first, then pixel 2 from row 2, pixel 3 from row 1, and so forth to create a horizontal output line that spatially averages between row 1 and row 2. The second line readout starts with pixel 1 from row 3, then pixel 2 from row 2, pixel 3 from row 3 and so forth to create a horizontal line that spatially averages between array row 2 and row 3. In this way a high-resolution image is created using all the horizontally polarized pixels twice. A vertically polarized image is also created using only the vertically polarized pixels and using each pixel twice.

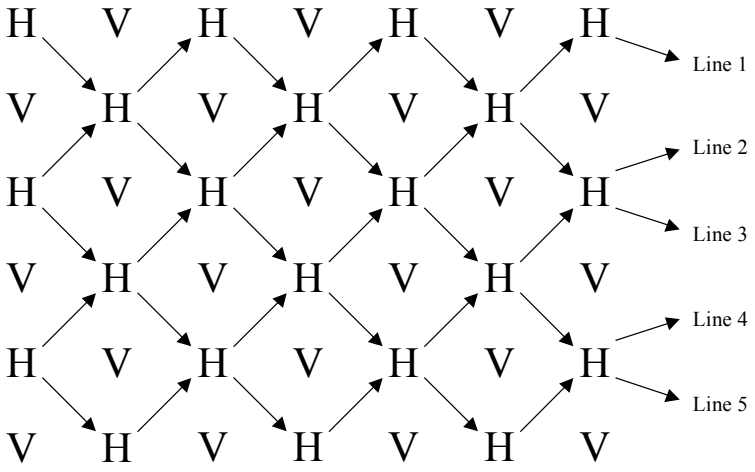

Figure 4. Schematic diagram of the readout scheme. H and V represent pixels sensitive to horizontally-polarized and vertically-polarized infrared radiation, respectively.

5. Imagery, Data, and Analysis

A preliminary analysis of this QWIP array was realized using data that was collected with the FPA operating in a pour fill dewar at 77°K. Once the FPA is installed in the camera system, the closed-cycle cooler can achieve operating temperatures down to 60 Kelvin or less.

These quantum well detectors are polarized which generally reduces the quantum efficiency by a factor of two. The normal conversion efficiency at this wave length is about 3 percent. Due to the polarization, we expect a conversion efficiency of only 1.5 percent. Conversion efficiency tends to remain a constant that is independent of the number of wells used in the quantum well.

Conversion efficiency is the product of two terms: quantum efficiency and photoconductive gain. The quantum efficiency of this quantum well detector is about seven percent due to the number of wells. The photoconductive gain should be about 0.2 electrons per electron for a forty-well structure operated at about 2 volts of bias. The photo conductive gain is a function of the applied bias voltage. It can be calculated based on the noise performance of the system.

The noise measurements can be analyzed using the photocurrent and thermionic leakage currents. Using the characteristics of the system, the characteristics of the quantum well can be deduced.

LWIR quantum well detectors need about to operate at a temperature that is about ten Kelvin less than their mercury cadmium telluride counterparts. This is because the leakage current is thermionically

limited. For a QWIP with peak wavelength of 9 μm operating at 77 Kelvin, the expected leakage current density for a 9.1 micron peak quantum well is about 1.4 mA/cm^2. Given a 3 μm ditch and a 40 μm pitch for our focal plane array, the fill factor is 85%. So the expected thermionic leakage current in our quantum well detector should be about 19.2 nA per pixel. This correlates well with laboratory pour fill dewar measurements which recorded a leakage current of 23 nA for a non-cold-shielded measurement.

Photo Current

The first item in any analysis is usually the calculation of the expected photocurrent. This calculation depends on a number of factors. The fundamental expression for the photocurrent is

$$i_p(T) = \frac{\tau\Omega A\eta q 2c\lambda_B}{\lambda_p^4} \exp(-hc/(kT\lambda_p)) \quad \text{Amperes}$$

where λ_p is the peak wave length	9.1 μm
λ_B is the spectral band pass	0.6 μm
τ is the optical transmission efficiency	0.5
Ω is the solid angle	0.196 sr (limited by the dewar)
η is the conversion efficiency	0.015 electrons/photon
A is the effective detector area	$13.69 * 10^{-6}$ cm^2
q is electron charge	$1.602 * 10^{-19}$ coulombs per electron
h is Planck's constant	$6.626 * 10^{-34}$ J-s
c is the velocity of light	$2.9979 * 10^{8}$ m/s
T is the target temperature in Kelvin	

To find the photocurrents we work backwards in the system. First, we measure the contrast in the analog-to-digital converter (ADC) which is 2.272 counts per Kelvin. The sensitivity of the converter is 1.22 mV/K, which gives 2.773 mV/K. There is an analog preamplifier in the laboratory set up that has a voltage gain of ten V/V. With the input of the preamplifier grounded there is less than one count of noise in the ADC's output so this system may be treated as noiseless. The contrast voltage at the output of the readout integrated circuit is 277 μV/K. The on-plane operational amplifier has a voltage gain of 2 V/V. So the noise at the output of the cell buffer amplifier is 138.6 μV/K. The cell buffer amplifier has an insertion loss of 0.83 V/V. So the contrast on the hold capacitor is 167 μV/K. The charge sharing loss of the hold and charge well transfer is 0.5 V/V, so the contrast at the charge well is 334 μV/K. Using the transfer resistance of 140 MΩ, there is a contrast current in the quantum well of 2.38 pA/K. Working backwards on the contrast produces a photocurrent of 207 pA. We know that the transmission efficiency of the dewar window and the optical lens system is 0.5, so given a 0.196 sr solid angle, the conversion efficiency of 0.015 electrons per photon is verified.

The noise analysis produces the value for the photoconductive gain. The noise at the analog to digital converter is 3.71 counts or 4.526 mV. Through the preamplifier this noise becomes 453 μV rms at the output of the focal plane. On the plane, and at the input to the operational amplifier the noise is 226

μV rms. The hold capacitor holds 272 μV rms of noise. The hold capacitor has a randomness of 272 μV rms. The charge well produces 545 μV rms or 3.90 pA of noise. The square root of the sum of squares of the noise from the hold capacitor, the input operational amplifier, and the hold capacitor, the total noise contribution is 341 μV at the charge well. Reversing the root mean square argument and extracting the photoconductive gain produces a value of 0.178 for the photoconductive gain which is very close to the 0.2 electrons per electron expected. The generation-recombination noise expression used in the above analysis was

$$\langle i_n \rangle = (4\beta q I_D f_n)^{1/2} \qquad \text{Amps rms}$$

where β is the photoconductive gain.

We are now in a position to evaluate virtually any system performance because we have extracted the model for the quantum well detector.

Quantum Well Model

Based on the reverse modeling process we have deduced the following model for the polarized quantum well detectors in the array.

Peak wavelength	9.1 μm
Passband	0.6 μm
Photoconductive gain	0.196
Quantum Efficiency	0.084 electrons/photon
Sigma/mean	0.03
Responsivity	0.108 A/W
Leakage Current Temperature Coefficient	8.50 Kelvin/decade

If we operate this quantum well at about 60 Kelvin, the leakage current drops by a factor of 100. If we operate this detector in an f/2 optical system with an optical transmission efficiency of 80% then we would have a 300 Kelvin background photocurrent of 136 pA and the system achieves background limited performance (BLIP). For this case, a 2 pF charge well capacitor is half filled at 12.8 ms and the noise equivalent delta temperature decreases into the single-digit mK regime.

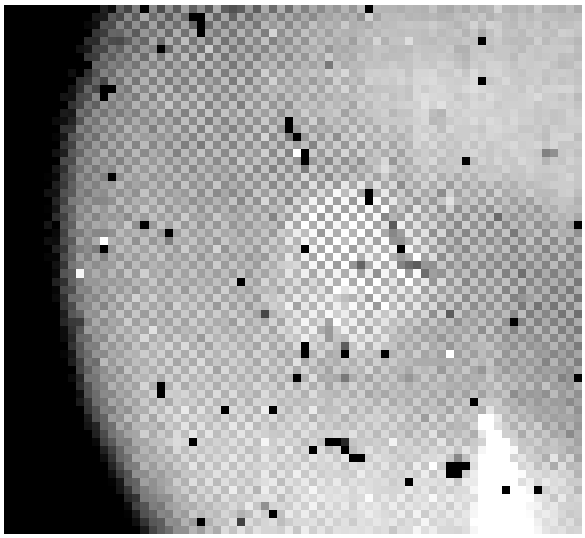

Figure 3. Image of a hot soldering iron, looking down at the tip and at grazing incidence along the cylindrical sleeve. The strong checkered pattern demonstrates

An image taken with the detector in the pour fill set up is shown in Fig.3. This image is of a hot curved cylinder (soldering iron sleeve). On the curved surface a clear pattern of alternating pixels is displayed. This pattern shows a polarization effect is present in this object.

6. Conclusions

We have fabricated a polarization-sensitive infrared camera based on a QWIP FPA with orthogonal gratings on adjacent pixels. This design eliminates the need to align polarization elements to pixel elements and therefore eliminates the associated mis-registration errors. The

The preliminary imagery gives a qualitative indication of the polarization performance of this instrument. Ongoing measurements will fully characterize the instrument and allow collection of field data.

Future work could include modifying the processing mask to include grating orientations of 0°, 45°, 90°, and 135° in a 2 x 2 pixel unit cell to quantify both the degree of linear polarization and the polarization angle. The FPA fabrication steps would be the same, and the electronics could be easily modified to read out four sub-images – one for each grating orientation.

7. Acknowledgements

The authors thank L. Lucas and K. Olver at ARL for FPA processing. Mr. Lane and Dr. Martin at ADIC for detector analysis. This work was conducted by Digital Imaging under SBIR contract F08630-97-C-0021 administered by Mr. David Hayden, WL/MNGS, Eglin AFB, FL.

8. References

1. K.P. Bishop, H.D. McIntire, M.P. Fetrow, and L. McMackin, “Multispectral polarimeter imaging in the visible to near-IR,” in *Targets and Backgrounds: Characterization and Representation V*, Proceedings of the SPIE, vol. 3699, pp. 49-57 (1999).
2. C.S.L. Chun, D.L. Fleming, W.A. Harvey, and E.J. Tork, “Polarization-Sensitive Thermal Imaging Sensor,” in *Infrared Technology XXI*, Proceedings of the SPIE, vol. 2552, pages 438 – 444 (1995).
3. J.R. Maxwell and T.J. Rogne, “Polarization”, Technote 97-01 in IRIA newsletter Spectral Reflections, Jan 97, and “Polarization II”, Technote 97-04, Spectral Reflections, Oct 97. Available at the IRIA website: http://csdnta.erim-int.com/iria/iriaweb.nsf
4. J.A. Shaw and M.S. Descour, “Instrument effects in polarized infrared images,” Opt. Eng. vol. 34, PP 1396 – 99 (May 1995).
5. B.F. Levine, "Quantum-well infrared photodetectors", J. Appl. Phys. vol. 74 (8), R1-R81 (1993).
6. S.D. Gunapala and K.M.S.V. Bandara, "Recent Developments in Quantum-Well Infrared Photodetectors*", Thin Films* **21**, 113-236 (1995).
7. K.K. Choi, *The Physics of Quantum Well Infrared Photodetectors*, World Scientific, New Jersey, (1997).